Inorg. Chem. **2007**, *46*, 2556–2562

Structure and Thermoelectric Characterization of $A_xBa_{8-x}Al_{14}Si_{31}$ (A = Sr, Eu) Single Crystals

Cathie L. Condron and Susan M. Kauzlarich*

Department of Chemistry, University of California Davis, One Shields Avenue, Davis, California 95616

G. S. Nolas

Department of Physics, University of South Florida, Tampa, Florida 33620

Received November 7, 2006

Single crystals of $A_xBa_{8-x}Al_{14}Si_{31}$ (A = Sr, Eu) were grown using a molten Al flux technique. Single-crystal X-ray diffraction confirms that $A_xBa_{8-x}Al_{14}Si_{31}$ (A = Sr, Eu) crystallize with the type I clathrate structure, and phase purity was determined with powder X-ray diffraction. Stoichiometry was determined to be $Sr_{0.7}Ba_{7.3}Al_{14}Si_{31}$ and $Eu_{0.3}Ba_{7.7}Al_{14}Si_{31}$ by electron microprobe analysis. These $A_xBa_{8-x}Al_{14}Si_{31}$ phases can be described as framework-deficient clathrate type I structures with the general formula, $A_xBa_{8-x}Al_ySi_{42-3y/4}[]_{4-1/4y}$. DSC measurements indicate that these phases melt congruently at 1413 and 1415 K for $Sr_{0.7}Ba_{7.3}Al_{14}Si_{31}$ and $Eu_{0.3}Ba_{7.7}Al_{14}Si_{31}$, respectively. Temperature-dependent resistivity indicates metallic behavior, and the negative Seebeck coefficient indicates transport processes dominated by electrons as carriers. Thermal conductivity of these phases remains low with $Sr_{0.7}Ba_{7.3}Al_{14}Si_{31}$ having the lowest values.

Introduction

Compounds with the type I clathrate structure continue to be of fundamental scientific interest for thermoelectric applications because they exhibit glass-like thermal conductivity, high electrical conductivity, and high Seebeck coefficients resulting in a high dimensionless figure of merit $zT = S^2T/\rho\kappa$.[1−4] In addition, there are a large number of isostructural clathrate phases that can use different combinations of elements in both the cages and framework sites. This potentially allows for the composition to be adjusted for a maximum zT value at a specific temperature range. Furthermore, clathrate phases have the added advantage of using light elements to form low-density thermoelectric materials, providing new materials for transportation applications. Light-element-containing compounds fall outside the accepted criteria for finding good thermoelectric materials and are therefore generally ignored for thermoelectric application.

However, clathrate phases provide an exciting avenue to obtain light element phases for thermoelectric applications due to their inherently low lattice thermal conductivity which is achieved by adopting a cagelike crystal structure.[5] Thus, a good light element thermoelectric material may be obtained by starting with a light element clathrate framework of Si/Al and systematically tuning the electronic properties. The Al−Si clathrate phases are attractive candidates not only because they offer a light element alternative to the Ga−Ge phases but also because they are expected to exhibit higher melting points than the Ga−Ge phases, thereby expanding the temperature regime where these phases may be applicable.

Thus far we have presented the synthesis, structure, Raman spectroscopy, and magnetism of Ba/Eu Al−Si-containing clathrate phases,[6] as well as the single-crystal neutron

* To whom corrrespondence should be addressed. E-mail: smkauzlarich@ucdavis.edu. Phone: (530) 752-4756. Fax: (530) 752-8995.

(1) Nolas, G. S.; Slack, G.; Schujman, S. B. In *Semiconductors and Semimetals*; Academic: San Diego, 2001; Vol. 69, p 225m and references therein.
(2) Blake, N. P.; Latturner, S.; Bryan, J. D.; Stucky, G. D.; Metiu, H. *J. Chem. Phys.* **2001**, *115*, 8060.
(3) Kuznetsov, V. L.; Kuznetsova, L. A.; Kaliazin, A. E.; Rowe, D. M. *International Conference on Thermoelectrics* **1999**, *18th*, 177.
(4) Blake, N. P.; Mollnitz, L.; Stucky, G. D.; Metiu, H. *International Conference on Thermoelectrics* **1999**, *18th*, 489.
(5) Schujman, S. B.; Nolas, G. S.; Young, R. A.; Lind, C.; Wilkinson, A. P.; Slack, G. A.; Patschke, R.; Kanatzidis, M. G.; Ulutagay, M.; Hwu, S. J. *J. Appl. Phys.* **2000**, *87*, 1529.
(6) Condron, C. L.; Porter, R.; Guo, T.; Kauzlarich, S. M. *Inorg. Chem.* **2005**, *44*, 9185.

10.1021/ic062115v CCC: $37.00
Published on Web 02/07/2007

diffraction, MAS NMR, and thermoelectric properties of $Ba_8Al_{14}Si_{31}$.[7] The single-crystal neutron refinement of $Ba_8Al_{14}Si_{31}$ showed that Al and Si share every framework site, with Al preferentially filling the 6c site. ^{27}Al MAS NMR provided further support for the Al site preference. The Seebeck coefficient, resistivity, and thermal conductivity data obtained at 300 K, taken together, yield a zT for $Ba_8Al_{14}Si_{31}$ of 0.010 which is fairly low; however, it should be possible to improve these values by doping smaller atoms into the guest sites. Guest−host interactions should be diminished with the smaller guest atoms, thus causing the thermal conductivity to decrease, resulting in an improved zT.[2,4,8−13] Additionally, we have also investigated the synthesis of $Ba_8Al_{14}Si_{31}$ and $EuBa_7Al_{13}Si_{33}$ by solid-state synthesis, and high-temperature thermoelectric properties were measured which show promising results that yielded reasonable zT values for $Ba_8Al_{14}Si_{31}$ with a maximum of 0.35 at 1150 K.[14] This promising zT value lends support to the importance of optimizing these phases further.

This paper presents single-crystal X-ray diffraction studies for $Sr_{0.7}Ba_{7.3}Al_{14}Si_{31}$ and $Eu_{0.3}Ba_{7.7}Al_{14}Si_{31}$. The structures of $Sr_{0.7}Ba_{7.3}Al_{14}Si_{31}$ and $Eu_{0.3}Ba_{7.7}Al_{14}Si_{31}$ are compared with $Ba_8Al_{14}Si_{31}$. Microprobe analysis and density measurements provide stoichiometry. TGA/DSC data indicate that $Sr_{0.7}Ba_{7.3}Al_{14}Si_{31}$ and $Eu_{0.3}Ba_{7.7}Al_{14}Si_{31}$ melt congruently at 1373 and 1372 K, respectively. The resistivity, Seebeck coefficient, and thermal conductivity as a function of temperature for $Sr_{0.7}Ba_{7.3}Al_{14}Si_{31}$ and $Eu_{0.3}Ba_{7.7}Al_{14}Si_{31}$ are also provided and compared with $Ba_8Al_{14}Si_{31}$. On the basis of the comparison between these phases, important trends have been noted to aid in further properties optimization.

Experimental Section

Synthesis. $Sr_{0.7}Ba_{7.3}Al_{14}Si_{31}$ was synthesized from the elements Ba (Johnson Matthey, 99.9%), Sr (Alfa AESAR, 99%), Si (AESAR, 99.999%), and Al (Matheson Colemen and Bell 99.6%) using the high-temperature metallic solution growth method.[15,16] All preparations were performed in a nitrogen-filled dry box with water levels less than 1 ppm. Large single crystals (1−60 mg) of $Sr_{0.7}Ba_{7.3}Al_{14}Si_{31}$ were grown using the ratio 2Sr:2Ba:30Si:70Al, and scaled to 1 g of Al. Other elemental ratios were tried in order to obtain a Sr-only or 1:3 Sr/Ba clathrate phase. However, these ratio changes resulted in no crystal growth for the case where Ba was included in the reactions and the Sr ratio was increased. This implies that for the formation of these clathrate phases via the flux method a certain amount of Ba must be present in order to stabilize the cage formation. When Ba was left out of the reaction mixture, the phase $SrAl_2Si_2$ was formed (confirmed by single-crystal and powder X-ray diffraction). The largest crystals were obtained from the reaction with a spinning temperature of 900 °C. Spinning temperatures of 800, 700, and 600 °C were also tried. At 800 °C, the crystal are slightly smaller, and at 700 and 600 °C, binary phases such as $BaAl_4$ and $SrAl_4$ were present in the product. Details of the general synthetic procedures for flux growth of Al−Si clathrates, as well as synthesis, microprobe, X-ray diffraction, and density measurements for $Ba_8Al_{14}Si_{31}$ and $Eu_{0.3}Ba_{7.7}Al_{14}Si_{31}$, have been reported previously.[6,7]

Microprobe Analysis. Single crystals of $Sr_{0.7}Ba_{7.3}Al_{14}Si_{31}$ and $Eu_{0.3}Ba_{7.7}Al_{14}Si_{31}$ were obtained from several different reactions, mounted in epoxy, and polished for subsequent analysis. A Cameca SX-100 electron microprobe equipped with five wavelength-dispersive spectrometers, operating at 10 nA current with a 20 keV accelerating potential was used for analysis. Net elemental intensities for Al and Si were determined with respect to pure elemental calibration standards that were polished before the measurement to ensure the elements were not oxidized. $SrBaNb_4O_{10}$, $BaAl_{3.54}Si_{0.41}$, and $EuPO_4$ were used as standards to determine the net elemental intensities for Ba, Sr, and Eu, respectively. Totals for all analyses were 100%, and the compositions were homogeneous within crystals, either within standard deviation or identical, when compared with crystals from different reactions. The compositions were determined to be $Sr_{0.74(0.05)}Ba_{7.26(0.03)}Al_{14.33(0.05)}Si_{30.66(0.05)}$ and $Eu_{0.287(0.03)}Ba_{7.712(0.36)}Al_{14.19(0.1)}Si_{31.18(0.11)}$ and will hereafter be referred to as $Sr_{0.7}Ba_{7.3}Al_{14}Si_{31}$ and $Eu_{0.3}Ba_{7.7}Al_{14}Si_{31}$.

Single-Crystal X-ray Diffraction. The single-crystal X-ray diffraction data for $Sr_{0.7}Ba_{7.3}Al_{14}Si_{31}$ and $Eu_{0.3}Ba_{7.7}Al_{14}Si_{31}$ were collected at ~90 K using a Bruker SMART 1000 CCD diffractometer employing graphite-monochromatized Mo Kα radiation (λ = 0.71069 Å). Data were collected in full sphere with 0.3° scans in ω and exposure times of 30s per frame. Lorentz and polarization effects were corrected for using the SAINT program, and absorption corrections were based on fitting a function to the empirical transmission surface as sampled by multiple equivalent reflections (program SADABS).[17] The structure solution was obtained by direct methods and refined by full-matrix least-squares refinement against F_0^2 using the SHELXTL 6.10 package.[17]

Density Measurements. The density of $Sr_{0.7}Ba_{7.3}Al_{14}Si_{31}$ and $Eu_{0.3}Ba_{7.7}Al_{14}Si_{31}$ was measured using the flotation method with the liquids CH_2I_2 (d = 3.31) and CH_2Cl_2 (d = 1.316). In the flotation method, the crystal is suspended in a mixture of liquids, one lighter and one heavier than the calculated density of the crystal. The proportions of the liquid are adjusted until the crystal remains suspended in the medium. The density of the liquid, determined by weighing a sample of known volume, is the density of the crystal.[18] Five different crystals for each compound were measured, and the average is reported.

Powder X-ray Diffraction. Powder X-ray diffraction data for $Sr_{0.7}Ba_{7.3}Al_{14}Si_{31}$ and $Eu_{0.3}Ba_{7.7}Al_{14}Si_{31}$ were collected with a Scintag PAD−V employing Cu Kα radiation. Data acquisition was performed with WinAcq software. Sample analyses and Rietveld refinement of selected samples were performed using the RIETICA software package. The peak profile was chosen to be pseudo-Voigt (Howard asymmetry), and the background was fit to a fifth-order

(7) Condron, C. L.; Martin, J.; Nolas, G. S.; Piccoli, P. M. B.; Schultz, A. J.; Kauzlarich, S. M. *Inorg. Chem.* **2006**, *45*, 9381.
(8) Cohn, J. L.; Nolas, G. S.; Fessatidis, V.; Metcalf, T. H.; Slack, G. A. *Phys. Rev. Lett.* **1999**, *82*, 779.
(9) Sales, B. C.; Chakoumakos, B. C.; Jin, R.; Thompson, J. R.; Mandrus, D. *Phys. Rev. B* **2001**, *63*, 245113/1
(10) Nolas, G. S.; Weakley, T. J. R.; Cohn, J. L.; Sharma, R. *Phys. Rev. B* **2000**, *61*, 3845.
(11) Blake, N. P.; Bryan, D.; Latturner, S.; Mollnitz, L.; Stucky, G. D.; Metiu, H. *J. Chem. Phys.* **2001**, *114*, 10063.
(12) Blake, N. P.; Latturner, S.; Bryan, J. D.; Stucky, G. D.; Metiu, H. *J. Chem. Phys.* **2002**, *116*, 9545.
(13) Blake, N. P.; Mollnitz, L.; Kresse, G.; Metiu, H. *J. Chem. Phys.* **1999**, *111*, 3133.
(14) Condron, C. L.; Gascoin, F.; Snyder, G. J.; Kauzlarich, S. M. *Chem. Mater.* **2006**, *18*, 4939.
(15) Canfield, P. C.; Fisk, Z. *Philos. Mag. B* **1992**, *65*, 1117.
(16) Kanatzidis, M. G.; Pottgen, R.; Jeitschko, W. *Angew. Chem.* **2005**, *44*, 6996.
(17) Sheldrick, G. M. *SADABS and SHELXTL*; Siemens Analytical X-ray Instruments, Inc.: Madison, WI, 1999.
(18) Stout, G. H.; Jensen, L. H. In *X-Ray Structure Determination, A Practical Guide*, 2nd ed.; John Wiley and Sons: 1989; p 89.

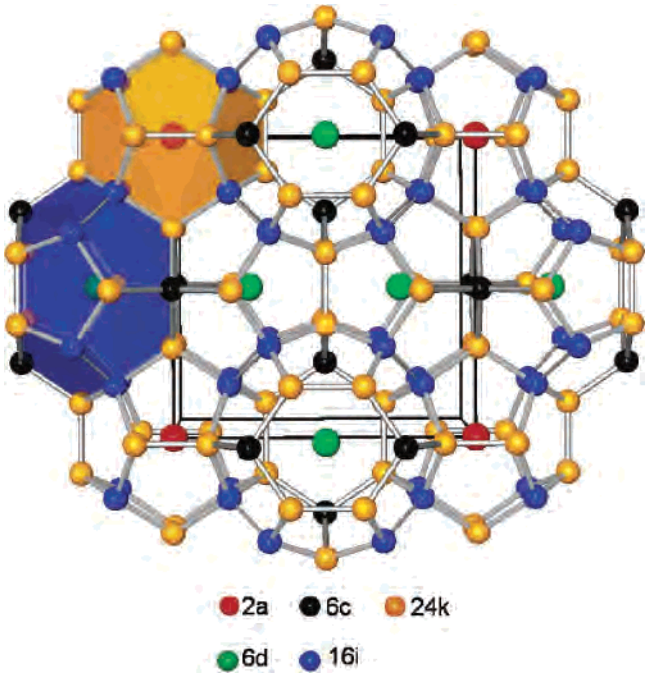

Figure 1. Polyhedral structure of the type 1 clathrate. Framework atoms are designated by color. The 6c sites are black, the 16i sites are blue, and the 24k sites are orange. The 2a sites are red, and the 6d sites are green. Crystal structure generated by *Balls and Sticks*.[33]

polynomial. Atomic positions, as well as the overall temperature factors, were held constant. The refinement for $Eu_{0.3}Ba_{7.7}Al_{14}Si_{31}$ has been previously reported.[6]

TGA/DSC. A Netzsch Thermal Analysis STA 409 STA, was used to evaluate the thermal properties of $Sr_{0.7}Ba_{7.3}Al_{14}Si_{31}$ and $Eu_{0.3}Ba_{7.7}Al_{14}Si_{31}$ between 400 and 1550 K. After a baseline was established, several crystals were ground into a powder (40−60 mg) which was placed in alumina crucibles and heated under argon at 10 K/min with an acquisition rate of 4pts/K. After the measurement, the samples were ground into powders and re-examined with powder X-ray diffraction.

Thermoelectric Properties Measurements. The crystals were cut with a wire saw, in order to minimize surface damage, in the shape of a parallelepiped $1 \times 1 \times 3$ mm^3 for transport measurements. The thermoelectric properties were performed similarly to that reported previously, however, with a few modifications.[19] Temperature-dependent four-probe electrical resistivity, and steady-state Seebeck coefficient and thermal conductivity measurements were simultaneously performed using a custom-designed closed-cycle refrigerator employing a differential thermocouple to measure the temperature gradient and 0.001 in. copper wires soldered to very small nickel-plated dots in the specimen for the voltage measurements.

Results and Discussion

Single-crystal X-ray diffraction studies confirmed that $Sr_{0.7}Ba_{7.3}Al_{14}Si_{31}$ and $Eu_{0.3}Ba_{7.7}Al_{14}Si_{31}$ crystallizes in the cubic space group $Pm\bar{3}n$ (Figure 1) with a unit cell edge of 10.5962(12) and 10.6306(12) Å, respectively. $Sr_{0.7}Ba_{7.3}Al_{14}Si_{31}$ has a smaller unit cell than $Ba_8Al_{14}Si_{31}$ (10.6246(12) Å) due to the smaller Sr cations replacing the larger Ba cations in crystal structure. If Eu completely replaced the Ba atoms in the crystal structure, it would be expected to have a smaller unit cell than both $Ba_8Al_{14}Si_{31}$ and $Sr_{0.7}Ba_{7.3}Al_{14}Si_{31}$. However, since there is only a small amount of Eu replacing the Ba in $Eu_{0.3}Ba_{7.7}Al_{14}Si_{31}$, the lattice parameter is not expected to change significantly. Tables 1−3 list the crystal data, structure refinement, atomic coordinates, and equivalent isotropic displacement parameters, and selected bond distances and angles for $Sr_{0.7}Ba_{7.3}Al_{14}Si_{31}$ and $Eu_{0.3}Ba_{7.7}Al_{14}Si_{31}$. For comparison, bond distances and angles for $Ba_8Al_{14}Si_{31}$ are also listed in Table 3.

Table 1. Crystal Data and Structure Refinement for $Sr_{0.7}Ba_{7.3}Al_{14}Si_{31}$ and $Eu_{0.3}Ba_{7.7}Al_{14}Si_{31}$

chemical formula[a]	$Sr_{0.7}Ba_{7.3}Al_{14}Si_{31}$	$Eu_{0.3}Ba_{7.7}Al_{14}Si_{31}$
space group	$Pm\bar{3}n$ (No. 223)	$Pm\bar{3}n$ (No. 223)
a (Å)	10.5962(12)	10.6306 (12)
V (Å^3)	1189.7(2)	1201.4(2)
Z	1	1
density (calcd)[a] (Mg/m^3)	3.170	3.286
abs coeff (mm^{-1})	7.532	7.643
θ range	2.72−28.16°	2.71−28.06°
reflns collected	12 372	8791
independent reflns	291 [R(int) = 0.0764]	291 [R(int) = 0.0361]
data/restraints/params	291/0/17	291/0/16
GOF on F^2	1.247	1.323
final R indices [$I > 2\sigma(I)$][b]	R1 = 0.0213 wR2 = 0.0432	R1 = 0.0142 wR2 = 0.0341
R indices (all data)	R1 = 0.0346 wR2 = 0.0503	R1 = 0.0153 wR2 = 0.0345
extincion coeff	0.0046(4)	0.0032(2)
largest diff. peak and hole (e·Å^{-3})	0.632 and −0.698	0.566 and −0.431

[a] Determined from microprobe analysis. [b] $R1 = [\sum||F_0| - |F_c||]/\sum|F_0|$; $wR2 = \{[\sum w[(F_0)^2 - (F_c)^2]^2]\}^{1/2}$; $w^{-1} = [\sigma^2(F_o) + (0.0471P)^2 + (0.5945P)]$ where $P = [\max(F_o^2,0) + 2F_c^{2/3}]$.

Similar to $Ba_8Al_{14}Si_{31}$ and $Eu_{0.3}Ba_{7.7}Al_{14}Si_{31}$, the framework bond lengths in $Sr_{0.7}Ba_{7.3}Al_{14}Si_{31}$ were not significantly different from each other; thus, bond length analysis could not be used to assign Al and Si to specific sites. However, recent neutron diffraction studies on $Ba_8Al_{14}Si_{31}$ indicate that Al preferentially fills the 6c site.[7]

Thus, the single-crystal X-ray diffraction data for $Sr_{0.7}Ba_{7.3}Al_{14}Si_{31}$ and $Eu_{0.3}Ba_{7.7}Al_{14}Si_{31}$ were evaluated according to the site occupancies provided by single-crystal neutron diffraction of $Ba_8Al_{14}Si_{31}$ for the framework sites.[7] The A/Ba occupancies were refined in the 2a sites giving site occupancies of 0.335/0.663 and 0.14/0.86 for Sr/Ba and Eu/Ba, respectively. This yields a total of 0.67 Sr and 7.326 Ba for $Sr_{0.7}Ba_{7.3}Al_{14}Si_{31}$ and 0.28 Eu and 7.72 Ba for $Eu_{0.3}Ba_{7.7}Al_{14}Si_{31}$. The framework-deficient model given here was verified by density measurements. Measured densities (flotation method) along with calculated densities for different elemental ratios are given in Table 4. The data are consistent with the defect model described above, although experimental density measurements are typically lower than the actual density of the sample.

From our single-crystal X-ray diffraction analysis, the M−M bond angles, where M is Al or Si, range from 105° to 124°, implying bonding that is similar to sp^3 hybridization in the diamond structure of Si and Ge. The M−M bond distances in $Sr_{0.7}Ba_{7.3}Al_{14}Si_{31}$ range from 2.388(3) to 2.497(1) Å and are slightly shorter than the bond distances in $Eu_{0.3}$-

(19) Martin, J.; Erickson, S.; Nolas, G. S.; Alboni, P.; Tritt, T. M.; Yang, J. *J. Appl. Phys.* **2006**, *99*, 044903.

Table 2. Atomic Coordinates and Equivalent Isotropic Displacement Parameters (U_{eq})[a] for $Sr_{0.7}Ba_{7.3}Al_{14}Si_{31}$ and $Eu_{0.3}Ba_{7.7}Al_{14}Si_{31}$ (M = Si/Al)

atom	site	*x*	*y*	*z*	U_{eq} (Å^2)	occ.
			$Sr_{0.7}Ba_{7.3}Al_{14}Si_{31}$			
Ba/Sr (1)	2a	0	0	0	0.0072(4)	0.663/0.335
Ba (2)	6d	0	0.25000	0.50000	0.0228(3)	1
M (1)	6c	0.25000	0	0.50000	0.0085(6)	0.44/0.55
M (2)	16i	0.18495(9)	0.18495(9)	0.18495(9)	0.0077(4)	0.70/0.27
M (3)	24k	0.11747(13)	0	0.30515(13)	0.0064(3)	0.70/0.27
			$Eu_{0.3}Ba_{7.7}Al_{14}Si_{31}$			
Ba/Eu(1)	2a	0	0	0	0.0059(2)	0.86/0.14
Ba(2)	6d	0	0.25000	0.50000	0.0183(2)	1
Si/Al (1)	6c	0.25000	0	0.50000	0.0082(3)	0.44/0.55
Si/Al (2)	16i	0.18491(6)	0.18491(5)	0.18491	0.0079(2)	0.70/0.27
Si/Al (3)	24k	0.11734(8)	0	0.30522(8)	0.0073(2)	0.70/0.27

Table 3. Selected Bond Lengths (Å) and Bond Angles (deg) for $Ba_8Al_{14}Si_{31}$, $Sr_{0.7}Ba_{7.3}Al_{14}Si_{31}$, and $Eu_{0.3}Ba_{7.7}Al_{14}Si_{31}$ (M = Si/Al)

bond lengths (Å)		bond angles (deg)	
		$Ba_8Al_{14}Si_{31}$	
Ba(1)−M(2)	3.4073(9)	M(2)−M(3)−M(1)	105.58(3)
Ba(1)−M(3)	3.4803(8)	M(2)−M(3)−M(2)	106.68(3)
Ba(2)−M(1)	3.7564(4)	M(2)−M(3)−M(3)	106.89(2)
Ba(2)−M(3)	3.5914(6)	M(2)−M(2)−M(3)	109.26(2)
M(1)−M(3)	2.4966(8)	M(3)−M(2)−M(3)	109.69(2)
M(2)−M(2)	2.3866(2)	M(3)−M(1)−M(3)	108.37(2)
M(2)−M(3)	2.4522(6)	M(3)−M(1)−M(3)	111.70(3)
M(3)−M(3)	2.5094(2)	M(1)−M(3)−M(3)	124.15(2)
		$Sr_{0.7}Ba_{7.3}Al_{14}Si_{31}$	
Ba/Sr(1)−M(2)	3.394(2)	M(2)−M(3)−M(1)	105.45(4)
Ba/Sr(1)−M(3)	3.465(2)	M(2)−M(3)−M(2)	106.60(6)
Ba(2)−M(1)	3.746(4)	M(2)−M(3)−M(3)	107.01(4)
Ba(2)−M(3)	3.582(1)	M(2)−M(2)−M(3)	109.33(5)
M(1)−M(3)	2.497(1)	M(3)−M(2)−M(3)	109.62(5)
M(2)−M(2)	2.388(3)	M(3)−M(1)−M(3)	108.44(3)
M(2)−M(3)	2.444(1)	M(3)−M(1)−M(3)	111.55(6)
M(3)−M(3)	2.489(3)	M(1)−M(3)−M(3)	124.22(3)
		$Eu_{0.3}Ba_{7.7}Al_{14}Si_{31}$	
Ba/Eu(1)−M(2)	3.405(1)	M(2)−M(3)−M(1)	105.43(3)
Ba/Eu(1)−M(3)	3.476(9)	M(2)−M(3)−M(2)	106.54(4)
Ba(2)−M(1)	3.759(4)	M(2)−M(3)−M(3)	107.03(2)
Ba(2)−M(3)	3.593(7)	M(2)−M(2)−M(3)	109.31(3)
M(1)−M(3)	2.505(9)	M(3)−M(2)−M(3)	109.63(3)
M(2)−M(2)	2.397(2)	M(3)−M(1)−M(3)	108.47(2)
M(2)−M(3)	2.453(7)	M(3)−M(1)−M(3)	111.48(4)
M(3)−M(3)	2.495(2)	M(1)−M(3)−M(3)	124.26(2)

Table 4. Calculated and Experimental Densities (mg/mL)[a]

stoichiometry	calculated	experimental
$Sr_{0.7}Ba_{7.85}Al_{13.5}Si_{29}$	3.034	
$Sr_{0.7}Ba_{7.3}Al_{14}Si_{31}$	3.218	3.21 (2)
$Sr_2Ba_6Al_{16}Si30$	3.16	
$Eu_{0.27}Ba_{7.22}Al_{13}Si_{29}$	3.057	
$Eu_{0.3}Ba_{7.7}Al_{14}Si_{31}$	3.239	3.24 (2)
$Eu_2Ba_6Al_{16}Si_{30}$	3.32	

[a] Experimental densities were performed using the flotation method with CH_2I_2 (d = 3.31), and CH_2Cl_2 (d = 1.316). Standard deviation from five crystals measured for each compound provided in parentheses.

$Ba_{7.7}Al_{14}Si_{31}$, which range from 2.397(2) to 2.505(9) Å. In comparison, $Ba_8Al_{14}Si_{31}$ has bond distances that range from 2.3866(2) to 2.5094(2) Å and are slightly larger than the bond distances found in $Sr_{0.7}Ba_{7.3}Al_{14}Si_{31}$ but on average shorter than those in $Eu_{0.3}Ba_{7.7}Al_{14}Si_{31}$. The minimum interatomic distances between the Ba ions and framework atoms in $Ba_8Al_{14}Si_{31}$ is 3.4073(9) Å [Ba(1)−M(2)], and the largest distance is 3.4803(9) Å [Ba(1)−M(3)]. The small differences between distances may provide a good fit for the Ba ion in the cage, resulting in an isotropically shaped thermal ellipsoid for the Ba ion. In contrast, the larger tetrakaidecahedron $(Al/Si)_{24}$ cage appears to be rather anisotropic, in agreement with our thermal parameters, with a minimum Ba(2)−M(3) distance of 3.4966(8) Å and a maximum Ba(2)−M(1) distance of 3.7564(4) Å. The anisotropy in this site suggests Ba(2) is interacting more strongly with the M(3) site, and although not addressed here, a split position model may be more suitable and is being investigated. Similarly, the minimum interatomic distances between the cations and framework atoms for $Sr_{0.7}Ba_{7.3}Al_{14}Si_{31}$ and $Eu_{0.3}Ba_{7.7}Al_{14}Si_{31}$ are 3.394(2) and 3.405(1) Å, respectively, for the small cage and 3.582(1) and 3.593(4) Å, respectively, for the large cage.

Powder X-ray diffraction experiments were used to determine phase purity, as well as room-temperature lattice parameters. Several clean crystals of $Sr_{0.7}Ba_{7.3}Al_{14}Si_{31}$ were selected and ground into sufficient particle size for powder X-ray diffraction analysis. Figure 2 shows the Rietveld profile fit for $Sr_{0.7}Ba_{7.3}Al_{14}Si_{31}$. It is clear from the diffraction pattern and corresponding fit that there were no obvious impurities in the $Sr_{0.7}Ba_{7.3}Al_{14}Si_{31}$ sample. The Rietveld refinement yielded a = 10.61710(5) Å, R_p = 9.233%, R_{wp} = 12.91%, χ^2 = 1.60, and R_{Bragg} = 1.8%. A similar analysis of $Eu_{0.3}Ba_{7.7}Al_{14}Si_{31}$ has been performed, and it also did not show impurities by Rietveld refinement.[6]

DSC scans for $Sr_{0.7}Ba_{7.3}Al_{14}Si_{31}$ and $Eu_{0.3}Ba_{7.7}Al_{14}Si_{31}$ are displayed in Figure 3. The powder X-ray diffraction patterns

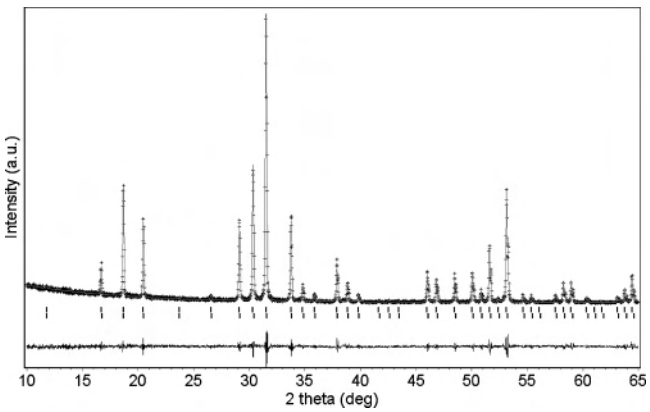

Figure 2. Rietveld profile fit for $Sr_{0.7}Ba_{7.3}Al_{14}Si_{31}$. Experimental data points are shown as black circles, and the theoretical fit is shown as a black solid curve. The data were refined for the space group $Pm\bar{3}n$ (black ticks), and the difference between the observed and theoretical patterns is shown below the black ticks. a = 10.61710(5) Å, R_p = 9.23%, R_{wp} = 12.91%, R_{Bragg} = 1.8%, χ^2 = 1.62.

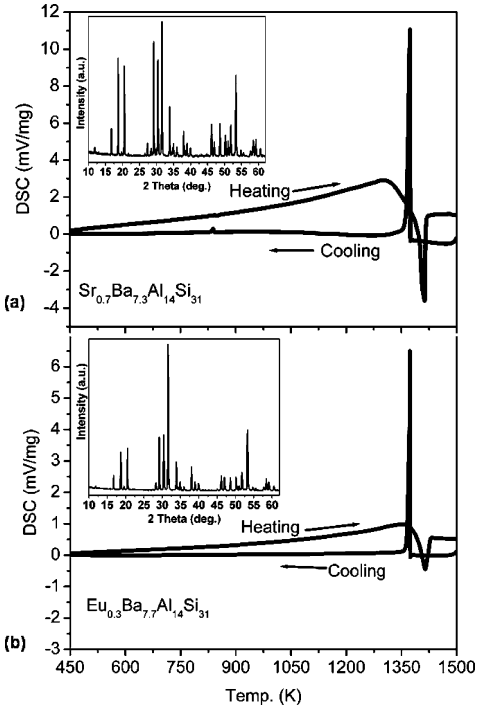

Figure 3. DSC (mV/mg) traces as a function of temperature for (a) $Sr_{0.7}Ba_{7.3}Al_{14}Si_{31}$ and (b) $Eu_{0.3}Ba_{7.7}Al_{14}Si_{31}$. Data were obtained by heating and cooling at a rate of 4 K/min under argon. Insets show the powder X-ray diffraction pattern after DSC.

after DSC experiments are shown as insets. Extra peaks in the powder X-ray diffraction can be attributed to slight oxidation of the sample at high temperatures. The DSC traces suggests that these phases melt (endotherm) at 1413 and 1415 K and recrystallize (exotherm) at 1373 and 1372 K for $Sr_{0.7}Ba_{7.3}Al_{14}Si_{31}$ and $Eu_{0.3}Ba_{7.7}Al_{14}Si_{31}$, respectively. There is no evidence for additional phase changes, with the exception of small amounts of Al that was not removed during the cleaning process. Moreover, there is no evidence of weight loss or weight gain in the TGA scans. Powder X-ray diffraction of the sample after melting is consistent with the original clathrate structure. Therefore, these clathrate phases melt congruently.

The temperature dependence of the electrical resistivity and Seebeck coefficient are shown in panels a and b of Figure 4, respectively. The data for the Ba phase have been previously reported but are presented here for comparison.[7] All three possess *n*-type conductivity, and the electrical resistivity increases with increasing temperature characteristic of metallic behavior. The absolute value of the Seebeck coefficient, $|S|$, gradually increases with increasing temperature with 25, 29, and 32 μV/K at 300 K for $Ba_8Al_{14}Si_{31}$, $Eu_{0.3}Ba_{7.7}Al_{14}Si_{31}$, and $Sr_{0.7}Ba_{7.3}Al_{14}Si_{31}$, respectively. Room-temperature Seebeck coefficient for the phase $Eu_2Ba_6Al_8Si_{36}$ was reported to be $\sim$7 μV/K[20,21] and is lower than the absolute value of the Seebeck coefficient for $Eu_{0.3}Ba_{7.7}Al_{14}Si_{31}$. Several trends emerge from comparing the data for $Ba_8Al_{14}Si_{31}$, $Eu_{0.3}Ba_{7.7}Al_{14}Si_{31}$, and $Sr_{0.7}Ba_{7.3}Al_{14}Si_{31}$. The most obvious trend is that with increased resistivity the absolute value of the Seebeck coefficient also increases. Also, by replacing some of the Ba with Sr, the resistivity increases. However, a similar effect is not observed for the Eu-substituted sample. Replacing some of the Ba with Eu causes the resistivity to decrease and the thermal conductivity to increase (discussed below). Since these samples can be considered heavily doped semiconductors, small differences in stoichiometry will make significant differences in resistivity. This has been seen in doping studies of semiconducting Ge clathrates.[22,23] Therefore, the trend $\rho_{Eu} < \rho_{Ba} < \rho_{Sr}$ cannot be simply rationalized on the basis of cation substitution; the carrier concentration is strongly dependent on vacancies and defects such that the vacancies and defects mask the intrinsic transport.

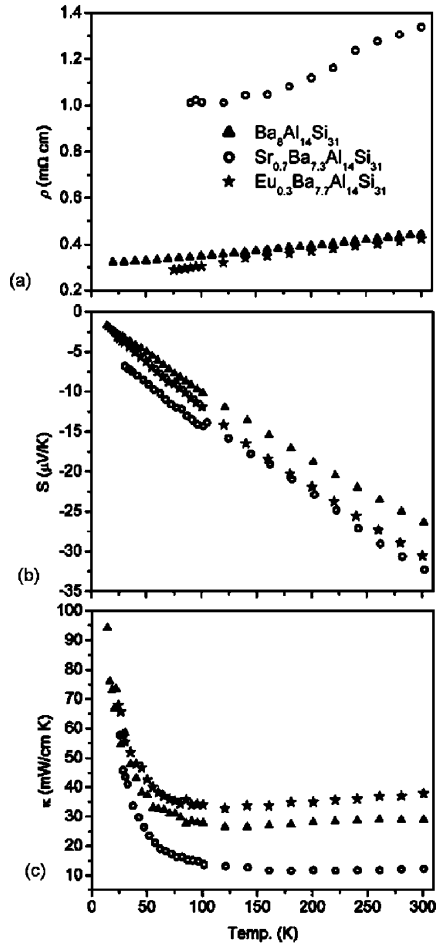

Figure 4. Temperature dependence of the (a) resistivity, (b) Seebeck coefficient, and (c) thermal conductivity for $Sr_{0.7}Ba_{7.3}Al_{14}Si_{31}$ (open circles), $Ba_8Al_{14}Si_{31}$ (black triangles), and $Eu_{0.3}Ba_{7.7}Al_{14}Si_{31}$ (black stars).

There are two components to the thermal conductivity. The electronic component (κ_e) depends on the electrical conductivity and can be estimated using the Wiedemann–Franz law, $\kappa_e = L_0T(1/\rho)$, where L_0 is the Lorenz number ($L_0 = 2.44 \times 10^{-8}$ W·Ω/K^2), ρ is the electrical conductivity,

(20) Mudryk, Y.; Rogl, P.; Paul, C.; Berger, S.; Bauer, E.; Hilscher, G.; Godart, C.; Noel, H. *J. Phys.: Condens. Matter* **2002**, *14*, 7991.
(21) Mudryk, Y.; Rogl, P.; Paul, C.; Berger, S.; Bauer, E.; Hilscher, G.; Godart, C.; Noel, H.; Saccone, A.; Ferro, R. *Physica B* **2003**, *328*, 44.
(22) Nolas, G. S.; Cohn, J. L.; Slack, G. A.; Schujman, S. B. *Appl. Phys. Lett.* **1998**, *73*, 178.
(23) Bryan, J. D.; Blake, N. P.; Metiu, H.; Stucky, G. D.; Iversen, B. B.; Poulsen, R. D.; Bentien, A. *J. Appl. Phys.* **2002**, *92*, 7281.

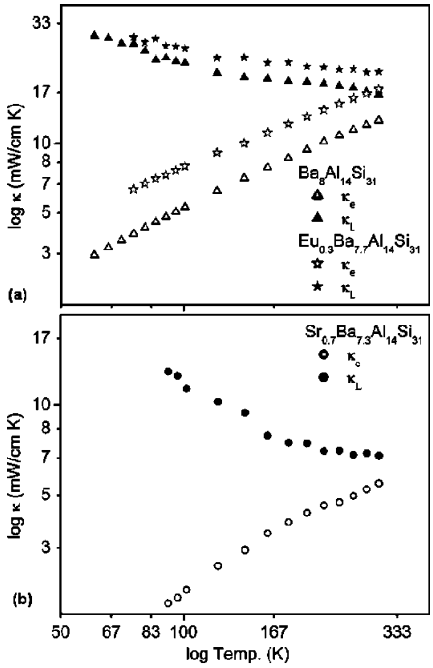

Figure 5. Log−log plots of temperature dependence of the (a) lattice (closed symbols) and electronic (open symbols) components of the thermal conductivity of $Ba_8Al_{14}Si_{31}$ (triangles) and $Eu_{0.3}Ba_{7.7}Al_{14}Si_{31}$ (stars) and (b) the lattice (closed symbols) and electronic (open symbols) component of the thermal conductivity for $Sr_{0.7}Ba_{7.3}Al_{14}Si_{31}$ (circles).

and T is temperature. The second component is the lattice component (κ_L) and depends on structural details and bonding. Figure 4c shows the total thermal conductivity for $Ba_8Al_{14}Si_{31}$, $Sr_{0.7}Ba_{7.3}Al_{14}Si_{31}$, and $Eu_{0.3}Ba_{7.7}Al_{14}Si_{31}$. $Ba_8Al_{14}Si_{31}$ and $Eu_{0.3}Ba_{7.7}Al_{14}Si_{31}$ have room-temperature thermal conductivity values that are larger than that of the Ga−Ge phases, likely due to the smaller, less massive framework atoms forming smaller, lighter polyhedra. $Sr_{0.7}Ba_{7.3}Al_{14}Si_{31}$ has the lowest thermal conductivity with a room-temperature value that is comparable to the Ga−Ge clathrate phases. Figure 5 shows the log of the lattice, κ_L (closed symbols), found by subtracting κ_e from κ, and electronic, κ_e (opened symbols), components to the thermal conductivity versus the log of the temperature for (a) $Ba_8Al_{14}Si_{31}$ and $Eu_{0.3}Ba_{7.7}Al_{14}Si_{31}$ and (b) $Sr_{0.7}Ba_{7.3}Al_{14}Si_{31}$. As shown in Figure 5, and observed in other type I silicon clathrates,[24] the electronic component to the thermal conductivity at room temperature for $Ba_8Al_{14}Si_{31}$ and $Eu_{0.3}Ba_{7.7}Al_{14}Si_{31}$ is nearly the same as the lattice component which is consistent with the metallic character of these phases. Although $Sr_{0.7}Ba_{7.3}Al_{14}Si_{31}$ has the lowest thermal conductivity, the temperature dependence of κ_L between 90 and 150 K is more similar to that of dielectric crystalline materials rather than amorphous phases. In crystalline materials, κ_L increases with decreasing T approximately as $1/T$ and is a signature of propagating phonons scattered by anharmonic interactions (phonon−phonon scattering).[25] The $1/T$ dependence observed for $T < 90$ K is also observed for the Ga−Si clathrate phases, as well as for Cs_8Sn_{44}, although the slopes are not the same.[26] For $Ba_8Al_{14}Si_{31}$ and $Eu_{0.3}Ba_{7.7}Al_{14}Si_{31}$, κ_L also increases with decreasing T, but not as strongly due to additional scattering at low temperatures.

As with many other clathrate phases, the lattice thermal conductivity is greatly affected by the degree of hybridization of the guest atom to the framework.[2,12,13,27−32] It has been shown experimentally and theoretically that by replacing larger guest atoms with smaller guest atoms the thermal conductivity of ternary clathrate phases decreases. This is explained by the fact that the smaller atoms are more loosely bound to the framework and can therefore scatter heat-carrying phonons more effectively.[2,4,8−13] This is consistent with $Sr_{0.7}Ba_{7.3}Al_{14}Si_{31}$ having a lower thermal conductivity than $Ba_8Al_{14}Si_{31}$ and having the smallest lattice contribution to κ.

Although Eu is smaller than Ba, the thermal conductivity of $Eu_{0.3}Ba_{7.7}Al_{14}Si_{31}$ is higher than that of $Ba_8Al_{14}Si_{31}$. The higher thermal conductivity of $Eu_{0.3}Ba_{7.7}Al_{14}Si_{31}$ was unexpected since it is known that Eu-doped Ga/Ge framework clathrate phases exhibit lower thermal conductivity than their Ba and Sr counterparts.[8−10] These reports are, however, on Ga/Ge clathrate phases that are fully occupied with Eu and Sr and have nominal framework stoichiometry, such as $Eu_8Ga_{16}Ge_{30}$ and $Sr_8Ga_{16}Si_{30}$. The lower thermal conductivity for both those phases has been attributed to a greater degree of nuclear distortion of the Sr and Eu atoms as determined by atomic displacement parameter (ADP) analysis of temperature-dependent neutron, synchrotron, or X-ray data.[8−10] In all studies, it was found that both the Eu and Sr in the fully occupied Ga/Ge phases have a broader (more spread out) nuclear density than the nuclear density of Ba in the Ga/Ge framework clathrate phases, with Eu having the highest degree of broadening or distortion.[1] Thus, the thermal conductivity for the Ga/Ge phases follows the trend $\kappa_{Ba} > \kappa_{Sr} > \kappa_{Eu}$. $Eu_{0.3}Ba_{7.7}Al_{14}Si_{31}$ is an anomaly compared with the Ga/Ge phases because it has the lowest resistivity and the highest thermal conductivity. The disorder on the cation site and the vacancies on the framework will both have a substantial affect on κ_L, making it difficult to assign the trend in κ_L to one specific effect. However, the larger disorder on the cation site for $Sr_{0.7}Ba_{7.3}Al_{14}Si_{31}$ as compared to that of $Eu_{0.3}Ba_{7.7}Al_{14}Si_{31}$ should result in smaller $\kappa_L$for $Sr_{0.7}Ba_{7.3}Al_{14}Si_{31}$ and is consistent with our data. Similarly, the difference in framework vacancies prohibits a direct comparison of κ_L of $Ba_8Al_{14}Si_{31}$ with that of $Eu_{0.3}Ba_{7.7}Al_{14}Si_{31}$ and $Sr_{0.7}Ba_{7.3}Al_{14}Si_{31}$.

In general, by increasing the resistivity, the absolute value of the Seebeck coefficient increases and the thermal con-

(24) Nolas, G. S.; Ward, J. M.; Gryko, J.; Qiu, L.; White, M. A. *Phys. Rev. B* **2001**, *64*, 153201/1.
(25) Berman, R. *Thermal Conductivity of Solids*; Clarendon Press: Oxford, UK, 1976.
(26) Nolas, G. S.; Chakoumakos, B. C.; Mahieu, B.; Long, G. J.; Weakley, T. J. R. *Chem. Mater.* **2000**, *12*, 1947.
(27) Reny, E.; San-Miguel, A.; Guyot, Y.; Masenelli, B.; Melinon, P.; Saviot, L.; Yamanaka, S.; Champagnon, B.; Cros, C.; Pouchard, M.; Borowski, M.; Dianoux, A. J. *Phys. Rev. B* **2002**, *66*, 014532/1.
(28) Nolas, G. S.; Kendziora, C. A.; Gryko, J.; Dong, J.; Myles, C. W.; Poddar, A.; Sankey, O. F. *J. Appl. Phys.* **2002**, *92*, 7225.
(29) Nolas, G. S.; Kendziora, C. A. *Phys. Rev. B* **2000**, *62*, 7157.
(30) Nolas, G. S. *Mater. Res. Soc. Symp. Proc.* **1999**, *545*, 435.
(31) Nataraj, D.; Nagao, J. *J. Solid State Chem.* **2004**, *177*, 1905.
(32) Iversen, B. B.; Palmqvist, A. E. C.; Cox, D. E.; Nolas, G. S.; Stucky, G. D.; Blake, N. P.; Metiu, H. *J. Solid State Chem.* **2000**, *149*, 455.
(33) Ozawa, T. C.; Kang, S. J. *J. Appl. Cryst.* **2004**, *37*, 679.

ductivity decreases, thus resulting in a larger zT. At 300 K, the zT for $Ba_8Al_{14}Si_{31}$, $Eu_{0.3}Ba_{7.7}Al_{14}Si_{31}$, and $Sr_{0.7}Ba_{7.3}Al_{14}Si_{31}$ is 0.013, 0.017, and 0.025, respectively. These are not unexpected, as similar values were found for $Ba_8Al_{16}Si_{30}$.[19,20] $Sr_{0.7}Ba_{7.3}Al_{14}Si_{31}$ is the most promising, and it would be worthwhile to explore higher Sr doping concentrations, along with measuring the thermoelectric properties at higher temperatures.

Summary

Single crystals of $Sr_{0.7}Ba_{7.3}Al_{14}Si_{31}$ were synthesized using the molten flux technique. Powder and single-crystal X-ray diffraction confirmed that $Sr_{0.7}Ba_{7.3}Al_{14}Si_{31}$ crystallizes with the clathrate type I structure. Stoichiometry was determined from microprobe data, and the phase purity was confirmed with powder X-ray diffraction. Although the zT values of these phases are low, we can make several important conclusions for the Al/Si framework clathrate phases: as the resistivity increases ($\rho_{Eu} < \rho_{Ba} < \rho_{Sr}$), the absolute value of the Seebeck coefficient increases ($S_{Ba} < S_{Eu} < S_{Sr}$) and the thermal conductivity decreases ($\kappa_{Eu} > \kappa_{Ba} > \kappa_{Sr}$). On the basis of these trends, it is conceivable that by systematically increasing the resistivity an optimal Seebeck coefficient and thermal conductivity may be achieved, resulting in a high zT light element thermoelectric material.

Acknowledgment. The authors gratefully acknowledge Dr. Alexandra Navrotsky (Department of Chemistry and Thermochemistry Facility and NEAT ORU, University of California Davis) for use of the Scintag powder diffractometer. This work was supported by the National Science Foundation (Grant No. DMR-0600742), and C.L.C. acknowledges a Tyco Electronics Foundation Fellowship in functional materials. G.S.N. thanks H. Rubin and J. Martin for help with transport measurements. G.S.N. acknowledges supported by the Department of Energy under Grant No. DE-FG02-04ER46145 for transport measurement analyses.

Supporting Information Available: Additional crystallographic data for $Sr_{0.7}Ba_{7.3}Al_{14}Si_{31}$ and $Eu_{0.3}Ba_{7.7}Al_{14}Si_{31}$ in CIF format. This material is available free of charge via the Internet at http://pubs.acs.org.

IC062115V